Total Ozone Column Changes over Northeast China: Trends and Variability Analysis

Yu Shi , Oleksandr Evtushevsky , Gennadi Milinevsky *

Posted Date: 17 March 2026

doi: 10.20944/preprints202603.1235.v1

Keywords: total ozone column; atmospheric temperature; Northeast China; MSR-2 dataset; quasi-stationary wave; stratosphere–surface coupling

 doi:10.20944/preprints202603.1235.v1

Article

Total Ozone Column Changes over Northeast China: Trends and Variability Analysis

Yu Shi [1], Oleksandr Evtushevsky [2] and Gennadi Milinevsky [3,4,5,*]

[1] College of Physical Science and Technology, Heilongjiang University, Harbin 150080, China
[2] Taras Shevchenko National University of Kyiv, Kyiv 01601, Ukraine
[3] College of Physics, International Center of Future Science, Jilin University, Changchun 130012, China
[4] Main Astronomical Observatory of National Academy of Sciences of Ukraine, Kyiv 01601, Ukraine
[5] National Antarctic Scientific Center, Kyiv 01601, Ukraine
* Correspondence: milinevskyi@jlu.edu.cn or genmilinevsky@gmail.com; Tel.: +86-150-4304-7624

Highlights

What are the main findings?

- Northeast China's total ozone column (TOC) is 25 DU higher than the zonal mean (winter-driven), peaks/troughs earlier than NH midlatitudes, and is governed by large-scale atmospheric processes ($r = 0.91$).
- The regional TOC is controlled by 50/100 hPa ozone, Longfengshan data matches MSR-2 well and shows strong stratosphere-surface coupling, plus a NE-SW TOC gradient in winter-spring.

What are the implications of the main findings?

- Northeast China is a key East Asian ozone transition zone, with winter-spring TOC regulated by QSW and BDC-linked transport, thereby defining the large-scale dynamic controls on regional midlatitude ozone.
- Validated Longfengshan data is a reliable TOC proxy, and the identified coupling/TOC patterns support East Asian midlatitude ozone-climate and stratosphere-troposphere research.

Abstract

Based on the Multi-Sensor Reanalysis Version 2 dataset, this study analyzes variations in monthly mean total ozone column (TOC) over Northeast China (40–53°N, 115–135°E) during 2015–2024. The study area in winter lies in the transition zone between high polar and low subtropical TOC in East Asian mid-latitudes. Key results indicate that the TOC over Northeast China is consistently higher than the zonal mean TOC of the same latitude band and seasonal cycle demonstrates TOC maximum (minimum) in February (August), one month (two months) earlier than for the Northern Hemisphere midlatitudes. The important role of Brewer–Dobson circulation and quasi-stationary wave (QSW) structure in the TOC distribution over Northeast China is confirmed by the 10-year climatology for January–March. The QSW pattern is characterized by the TOC decrease from the northeastern (~415 DU) to southwestern (~330 DU) parts of the region. The strongest positive (negative) correlations approaching $r = 0.9$ ($r = –0.8$) exist between TOC and ozone concentration (temperature) at 50 hPa and 100 hPa, as well as at the surface. These findings can be applied to analyze the ozone observations and stratosphere–surface couplings in the Northeast China region.

Keywords: total ozone column; atmospheric temperature; Northeast China; MSR-2 dataset; quasi-stationary wave; stratosphere–surface coupling

1. Introduction

Ozone is a critical component of the Earth's atmosphere, functioning as a natural barrier that efficiently absorbs harmful solar shortwave ultraviolet radiation (UV-B, 280–315 nm) [1]. Its

 doi:10.20944/preprints202603.1235.v1

variations directly regulate global climate systems, atmospheric circulation, and ecological balance, while profoundly impacting human health-excessive UV exposure is linked to increased risks of skin cancer and cataracts [2,3].

The Brewer–Dobson Circulation (BDC) is a quasi-steady meridional circulation centered in the stratosphere. It drives ascent in the tropical lower stratosphere, poleward transport and descent in the extratropical stratosphere, shaping the distribution of stratospheric tracers such as ozone and water vapor. Not radiatively driven, it relies on angular momentum from dissipating tropospheric waves including Rossby and gravity waves. Synoptic-scale Rossby waves dissipate in the subtropical lower stratosphere while planetary-scale ones dissipate in the winter polar vortex periphery. Both drive poleward flow via negative drag [4]. BDC intensification peaks in Northern Hemisphere (NH) winter months December, January and February (DJF) linked to stronger subtropical jet and wave drag changes, while summer months June, July and August (JJA) sees weaker wave activity and BDC due to the reversal of the zonal wind in the stratosphere from westerly to easterly [4–6].

In ozone depletion, BDC governs halogen residence time and polar ozone supply. The Antarctic vortex's chemical isolation depends on BDC's mixing barrier. Arctic ozone changes split evenly between BDC weakening and chemistry. Approximately 30% of 1979–2000 NH mid-latitude ozone decline relates to BDC transport. Seasonally, BDC-driven transport builds winter–spring ozone [6]. Summer photochemistry involving ozone-halogen reactions depletes it. An intensified BDC accelerates chlorofluorocarbons (CFC) removal and shifts ozone from tropics to mid-latitudes. This leads to tropical ozone decline and mid-latitude rise. The NH mid-latitudes may see ozone "super-recovery" exceeding CFC-induced losses by 2100 [4,6].

Geographically, ozone exhibits distinct latitudinal variations: near the equator, TOC is the lowest, yet near-surface ozone is the highest, with its vertical ozone peak occurring at a relatively high altitude (~25 km) and featuring a simple vertical structure [7]. In polar regions, total ozone reaches the highest level, while its peak altitude is relatively low (~20 km) and displays a complex multi-peak vertical structure; in mid-latitudes, both total ozone and vertical structure fall between those of the equatorial and polar regions [7,8]. Driving part of this distribution is the hemispheric BDC, which transports stratospheric ozone from its tropical source to the extratropics [9].

Tropical TOC variations exhibit distinct temporal phases, with TOC showing a strong negative trend before 1998 and most TOC trends becoming insignificant after 1998 (1979–2019 NOAA SBUV data); mid-stratospheric ozone continued to decline during the latter period, while near-surface ozone shifted from a negative to a positive trend [10]. High-latitude TOC is regulated by climatic indices, as evidenced by 2005–2021 OMI-derived TOC at three Norwegian sites: TOC variability at the high-latitude Andøya and Trondheim sites was dominated by the SCAND index, while TOC at Oslo showed weak correlations with NAO/AO; post-2016, the TOC-geopotential height correlation turned positive, and no significant TOC anomalies were observed at Oslo during periods of increased solar activity [11].

Since the discovery of the Antarctic ozone hole in 1985, ozone depletion and recovery have remained a core focus of the global environmental community [12]. In the late 20th century, widespread emissions of ozone-depleting substances (ODSs) such as CFCs caused significant global ozone layer thinning [8,13,14].

However, the global implementation of the Montreal Protocol and its amendments have effectively curbed ODS emissions, driving a gradual recovery of stratospheric ozone in mid-latitudes worldwide since the early 21st century [15–17]. Arctic springtime ozone depletion continues to weaken, with declining halogenated ozone-depleting substances (hODSs) as the dominant factor and limited GHGs impact. Future extreme Arctic ozone depletion events will drop notably, and the ozone layer overall shows a recovery trend in the models [18]. Recent observations indicate that upper stratospheric ozone in the NH mid-latitudes has exhibited a significant positive trend of 1–3% per decade during 2000–2024 [19]. The 2024 Antarctic ozone hole's area and depth are below long-term averages; with reduced ozone loss saturation since the 2000s, the layer is projected to recover to 1980s levels by mid-century [20].

 doi:10.20944/preprints202603.1235.v1

Global-scale stratospheric ozone research has laid a solid foundation for understanding macro patterns and core driving mechanisms. The slowing of the NH ozone depletion after 1998 significantly reduced the stratospheric cooling rate, highlighting the climate feedback effects of ozone changes [21]. Ozone variations regulate planetary wave activity and exert differential impacts on polar vortex intensity across the Northern and Southern Hemispheres [22]. Specifically, hemispheric differences exist in the impacts of quasi-stationary planetary waves (QSWs) on high-latitude TOC, with QSW 1 dominating in the Southern Hemisphere (SH) during spring across all analyzed years (1979–2003 TOMS data) and exhibiting the largest amplitude, though QSW 2 reached a comparable level in some NH years.

Maximal TOC disturbances induced by planetary waves occur in the winter–spring period in both the NH (January–March) and SH (August–October). During the development of the Antarctic ozone hole, the QSW phase at 60°N lacked the zonal motion observed at 60°S, and both hemispheres showed strong inter-annual variability in the position and amplitude of QSW patterns [23]. El Niño–Southern Oscillation modulates Antarctic ozone variability through teleconnection pathways, which enriches the understanding of large-scale climate–ozone interactions. Notably, global ozone recovery exhibits substantial regional heterogeneity, especially in East Asian mid-latitudes–a key transition zone between the polar high-ozone region and the tropical low-ozone region.

For East Asia and China, TOC variations exhibit unique characteristics, with ENSO exerting an impact on Chinese TOC: El Niño events increase Chinese TOC, while La Niña events reduce it, and maximum anomalies shift northward (south in winter, north in summer) linked to the East Asian westerly jet, causing 6–10% changes in clear-sky UV radiation [24]. TOC in East Asia showed an upward trend of ~1% per decade from 1997 to 2017, with TOC over the Korean Peninsula and Manchuria consistent with ground-based data (Seoul: 1.27% per decade; Pohang: 1.02% per decade), and atmospheric variability exerting a greater impact on TOC in 2020 [25]. Extreme TOC changes have been observed in the high-latitude Arctic, where Arctic TOC reached a 1979-record 477 DU in March 2024 (dominated by the lower stratosphere), driven by upward-propagating Rossby waves that warmed the stratosphere and enhanced poleward and downward ozone advection [26]. Rossby Wave Breaking (RWB) is a core process driving stratosphere–troposphere exchange in the NH, with significant differences in transport efficiency between RWB types [27]. Intense cutoff low events over East Asia trigger deep stratospheric intrusion via tropopause folding, elevating tropospheric ozone concentrations [28]. Subsequent studies further refined this understanding by linking RWB, the Northeast (NE) China Cold Vortex, and stratosphere-to-troposphere transport to surface ozone increases in eastern China [29,30].

Notably, SH sudden stratospheric warmings induce significant zonal asymmetry in Antarctic total ozone column, with stronger positive anomalies in the Eastern Hemisphere and weaker ones in the Western Hemisphere [31]. The NH polar vortex shift toward Eurasia regulates stratospheric ozone changes over the continent through a "dynamic + chemical" dual mechanism, and Eurasia may be one of the regions with the latest ozone recovery in the NH due to combined effects of ODS emission reduction and climate system changes [32]. The dynamic changes of the Arctic polar vortex impact mid-high latitude ozone distribution, but its specific role in Eurasian ozone loss remains unclear [32]. Under the high-emission (A1FI) scenario, future climate warming will alter stratosphere–troposphere ozone transport and tropospheric ozone lifetime, with upper tropospheric ozone showing significant increases and the stratospheric contribution to tropospheric ozone further enhancing [33].

On a national scale, TOC in China shows a slight downward trend with distinct temporal cycles and spatial patterns, and it is significantly correlated with anthropogenic emissions [34]. However, existing research on stratospheric ozone over NE China has obvious gaps: most studies either focus on surface ozone or cover only short-term periods [35–38], failing to address the critical 2015–2024 decade—a pivotal phase for global ozone recovery. As a key mid-high latitude region sensitive to polar vortex dynamics and stratosphere–troposphere exchange processes, the long-term trend, seasonal characteristics, consistency with global mid-latitude patterns, and key driving factors of the

 doi:10.20944/preprints202603.1235.v1

total ozone column in NE China remain insufficiently resolved [39]. This gap hinders a comprehensive understanding of regional ozone recovery dynamics and the linkage between large-scale climate processes and local ozone variability over the region.

This study focuses on the TOC over NE China (40–53°N, 115–135°E), which lies in the mid-latitude transition zone between the polar and subtropical latitudes and where stratospheric ozone dynamics are governed by large-scale atmospheric processes such as Brewer–Dobson circulation and mid-latitude circulation adjustments inherent in East Asia region. Using the Multi-Sensor Reanalysis Version 2 (MSR-2) dataset during 2015–2024, we aim to clarify the study region's TOC characteristics compared to the mid-latitude zone 40–53°N as a whole and provide baseline data for East Asian mid-latitude ozone dynamics. In what follows, Section 2 describes the dataset, study area, and analytical methods; Section 3 presents the key results of TOC variations; Section 4 provides a discussion, and Section 5 draws conclusions from the study.

2. Materials and Methods

2.1. Study Area

The study area covers Northeast (NE) China, defined by geographical coordinates of 40–53°N latitude and 115–135°E longitude, as shown in Figure 1. This region includes three provincial administrative regions (Liaoning, Jilin, Heilongjiang) and parts of Inner Mongolia Autonomous Region. Topographically, it features diverse landscapes, including plains, mountains, and plateaus, with an average elevation ranging from 50 to 1,500 meters above sea level. Climatologically, the region is dominated by a temperate continental monsoon climate, characterized by cold and dry winters and warm and humid summers. The distinct seasonal climate may influence stratospheric-tropospheric exchange processes and indirectly affect TOC distribution.

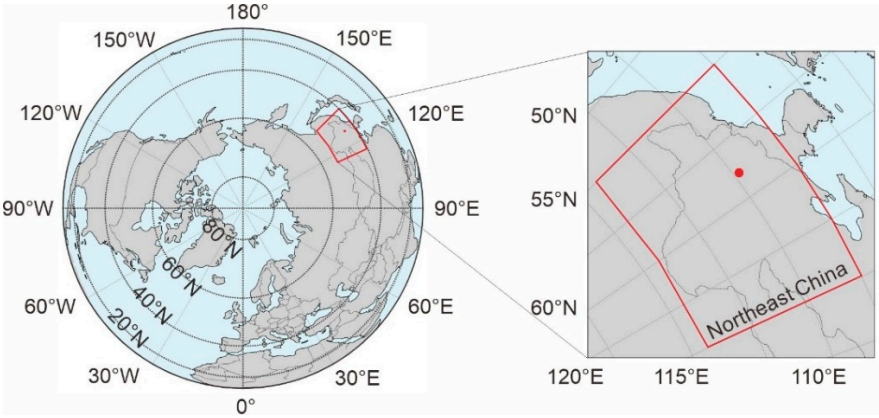

Figure 1. Map of the research area in Northeast China (40–53°N, 115–135°E), the red dot represents the Longfengshan Station (44.7°N, 127.6°E).

2.2. Data Source

The primary dataset utilized in this study is the Multi-Sensor Reanalysis Version 2 (MSR-2), a comprehensive Total Ozone Column (TOC) product integrating observations from multiple satellite sensors and ground-based measurements, with a temporal scope spanning 2015–2024 (the past 10 years) and consisting of monthly average data (120 time points in total), a spatial resolution of 0.5°×0.5°(latitude × longitude) that ensures sufficient spatial detail to capture regional variations over NE China, a focus on the TOC variable expressed in Dobson Units (DU), and strict quality control processes including noise reduction, sensor calibration, and cross-validation with independent observations that guarantee high reliability for long-term trend analysis [40].

Time–pressure profiles of ozone concentration and temperature are based on and ERA-5 reanalysis. Developed by the European Centre for Medium-Range Weather Forecasts (ECMWF),

 doi:10.20944/preprints202603.1235.v1

ERA-5 is a widely used global atmospheric reanalysis product with a horizontal resolution of 0.25°×0.25° (approximately 31 km at the equator) and coverage of 37 standard pressure levels, ranging from 1000 hPa (near the surface) up to 1 hPa (in the upper stratosphere). Its comprehensive pressure-level coverage and fine spatial resolution enable ERA-5 to effectively capture the vertical and temporal variations of ozone concentration and temperature in time-pressure profile analyses [41].

In addition, this study employs the TOC data from Longfengshan Station (marked as a red dot on the regional map in Figure 1b), a regional background station located in NE China (44.7°N, 127.6°E, 331 m a.s.l.), approximately 175 km NE of Harbin City. As a Regional Station of the Global Atmosphere Watch (GAW) under World Meteorological Organization (WMO) Region II (Asia) with GAW ID: LFS and WOUDC Station ID: 326, the station's data is publicly archived and accessible via the World Ozone and Ultraviolet Radiation Data Centre (WOUDC) platform (access link: https://woudc.org/en/data/stations/?id=326&lang=en), with data provision ceasing after March 2022. The dataset used in this study covers the period from January 2015 to March 2022. Managed by the Institute of Atmospheric Chemistry, Chinese Academy of Meteorological Sciences, the station's long-term observational records provide reliable data support for the analysis of regional ozone variability.

3. Results

In Section 3, we analyze the temporal trends, variability and climatology of TOC in the Northeast China using the MSR-2 data. Stratospheric ozone concentration and temperature relationships are derived from the ERA-5 dataset. The Longfengshan Station Brewer MKII data are used in comparison with TOC averaged over the NE China region.

3.1. Long-Term Trend of TOC

Figure 2 presents the 10-year (2015–2024) total ozone column time series over NE China (40–53°N, 115–135°E) and the zonal mean TOC across the same latitude band (40–53°N, 180°W–180°E). In Figure 2(a), blue filled circles denote the monthly mean TOC of NE China, while rose-red filled squares represent the zonal mean TOC. Figure 2(b) shows linear trends (dashed lines in corresponding colors) with semi-transparent shaded areas indicating 95% confidence intervals. All data are derived from HDF datasets, with non-physical values (< 0) excluded as NaN. Notably, the TOC over NE China shows no upward trend throughout the period, and it is consistently higher than the zonal mean TOC at the same latitude. The excess is about 25 DU (7.4%) and is contributed mainly by the higher winter TOC values in the NE China region than in the zonal means (blue and red symbols, respectively, at its maximum levels in Figure 2). The minimum TOC values in summer are close and do not affect the difference.

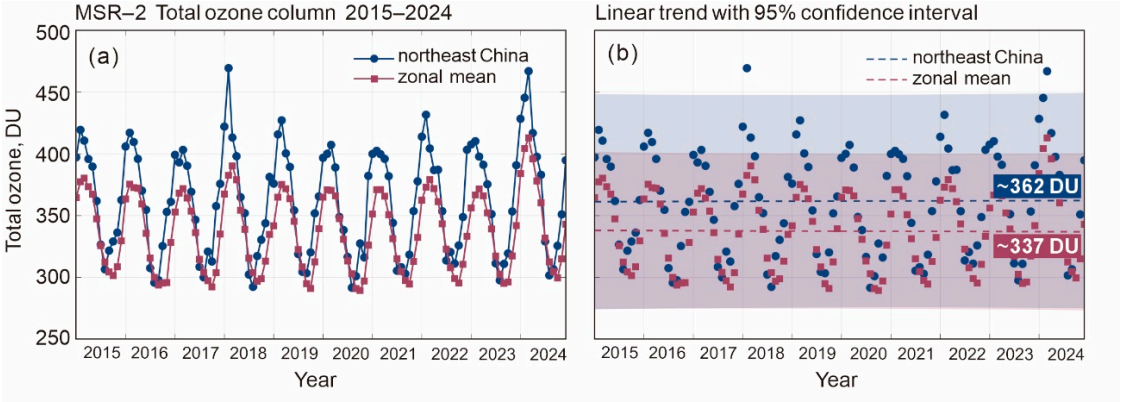

Figure 2. (a) Total ozone column in Northeast China and the full longitude band; (b) Linear trend with 95% confidence interval.

 doi:10.20944/preprints202603.1235.v1

Though the NE China's TOC lacks an upward trend, mathematical signal analysis reveals a strong positive correlation between the TOC variation signal of NE China and the full longitude band with $r = 0.91$. This consistency suggests that annual TOC dynamics in NE China is mainly dominated by zonal-scale atmospheric processes that reflected in regional processes. Subsequent work will focus on correlation characteristics across different latitude circles to further clarify the spatial consistency of ozone variations.

3.2. Seasonal Variability of TOC

Figure 3(a) presents the monthly variations of TOC in the NE China region from 2015 to 2024. The blue curves of different shades are monthly means for each year, red curve is 10-year monthly mean, and dashed line is 10-year annual mean. The overlapping blue curves show how monthly TOC varies between years, and notably, February 2018 and March 2024 stood out as periods of anomaly, a phenomenon that underscores the inherent instability of winter atmospheric dynamics and planetary waves [26]. The red curve highlights the consistent seasonal pattern of TOC over the decade with a maximum in February and a minimum in August, which are one month earlier and two months earlier, respectively, than usual in the NH midlatitudes [4].

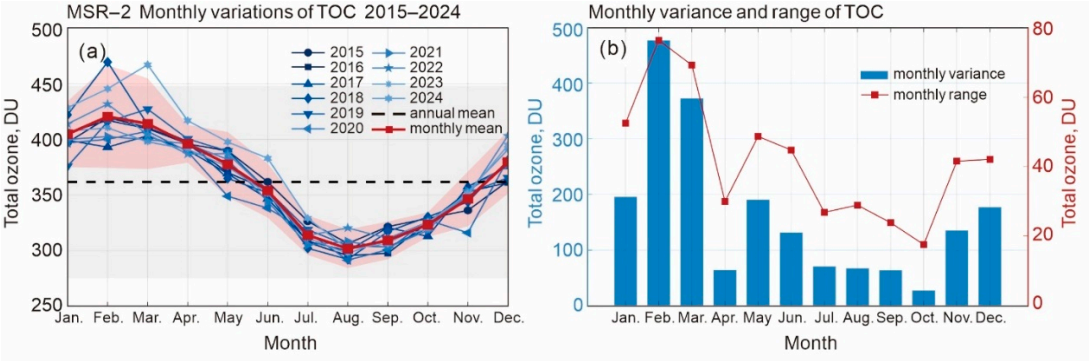

Figure 3. MSR-2 data for (a) Monthly variations of TOC during 2015–2024 (blue) with monthly mean (±2σ, red) and annual mean (±2σ, gray); (b) Monthly variance and range of TOC in the NE China region.

Figure 3(b) quantifies TOC's monthly volatility (variance s^2) and dispersion (range R) via a dual-Y-axis layout. The blue bar plot corresponds to the variance, which characterizes the temporal variability of monthly TOC values across the 10-year study period. The monthly sample variance is computed as:

$$s^2 = \frac{1}{9}\sum_{i=1}^{10}\left(x_i - \bar{x}\right)^2, \tag{1}$$

This variance exhibits a distinct peak in February, indicating substantial interannual variability in TOC during this month. Conversely, monthly TOC values exhibit minimal fluctuations during July, August, September, and October, resulting in comparatively low variance for these periods. The red curve, labeled "Range", quantifies the difference between the monthly maximum and minimum TOC values; mathematically, this range (denoted as R) is defined as:

$$R = \max\left(x_1, x_2, \ldots, x_{10}\right) - \min\left(x_1, x_2, \ldots, x_{10}\right), \tag{2}$$

Consistently with the variance pattern, the TOC range is notably larger across winter months, while it remains substantially smaller throughout the summer season.

Building on the prior analysis of long-term TOC trend and annual cycle (Figures 2 and 3), Figure 4 displays the monthly mean NH TOC spatial distribution across 2015–2024, organized by seasons: winter (December–February, a–c), spring (March–May, d–f), summer (June–August, g–i), and autumn (September–November, j–l). The red dashed box in each panel demarcates NE China. Mid-

 doi:10.20944/preprints202603.1235.v1

and high-latitude regions (≥40°N) exhibit elevated TOC values in winter and spring (a–f), while TOC decrease broadly in summer (g–i) before gradually recovering in autumn (j–l). Within this pattern, following Figure 3a, NE China (red box) shows relatively high TOC in winter and spring (Figure 4a–4f), transitions to low values in summer with minimum in July–September (Figure 4h–4j), and the regional TOC undergoes a partial rebound in autumn (October–November, Figure 4k and 4l).

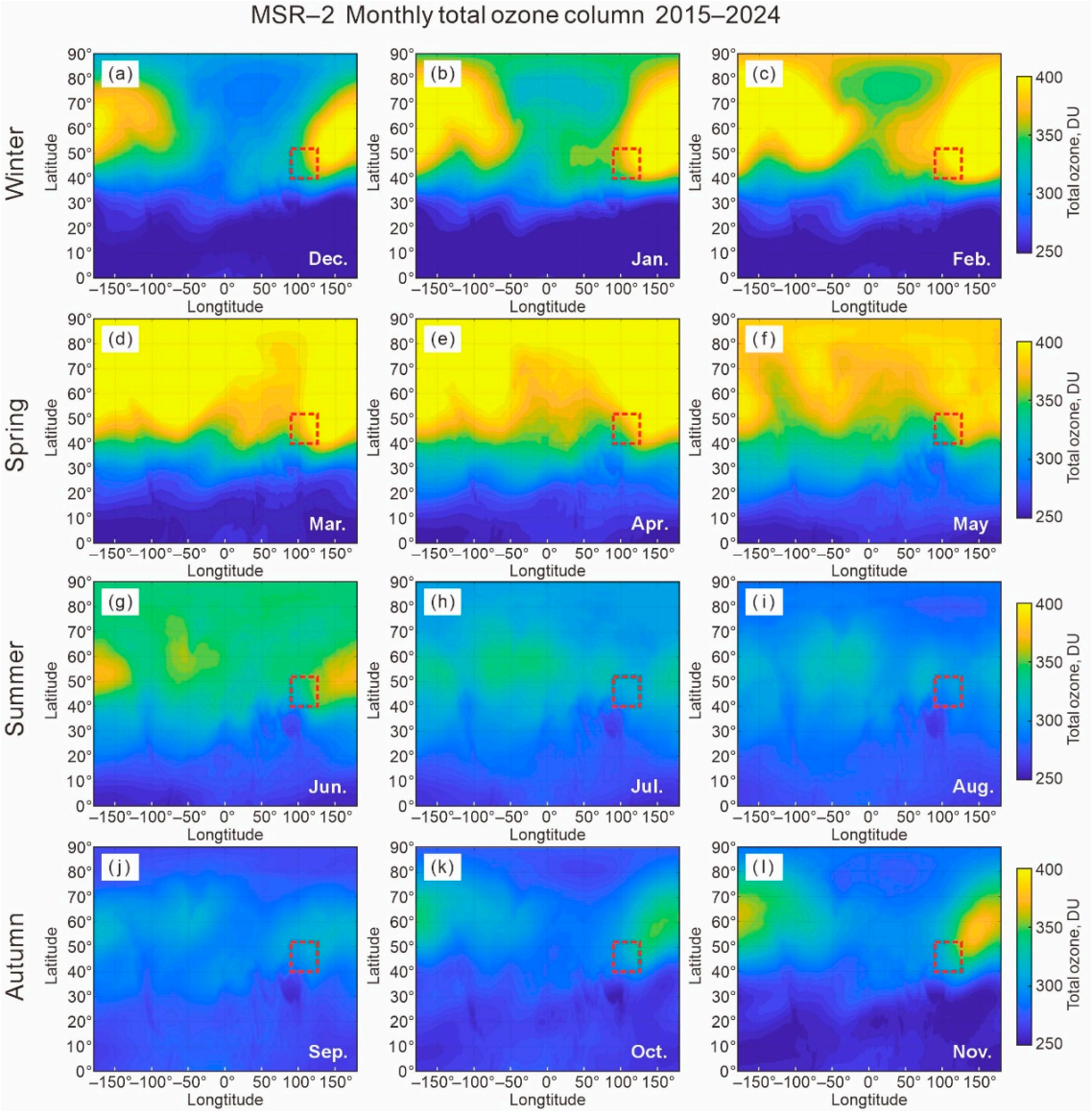

Figure 4. Total ozone column from 2015 to 2024, the red box indicates 40–53°N, 115–135°E in the Northeast China region.

This seasonal spatial pattern reveals that TOC in NE China aligns with typical mid-latitude ozone dynamics: higher winter/spring TOC tied to enhanced Brewer–Dobson circulation (BDC), and lower TOC in summer driven by increased photochemical destruction of stratospheric ozone and weaker transport [4]. Notably, the TOC minimum in NE China and in the 40–53°N latitude band does not differ in summer (Figure 2), indicating regional ozone levels are representative of mid-latitude conditions rather than extreme regional depletion. The spatial-temporal distribution of TOC in Figure 4 provides a foundational context for subsequent analyses of the large-scale atmospheric processes governing the NE China's ozone variability.

 doi:10.20944/preprints202603.1235.v1

3.3. 10-Year Climatology of TOC

Figure 5(a) presents the 2015–2024 climatology of TOC over the Northern Hemisphere for the JFM (January–March) season, with the TOC maximum over the NE China region (Figure 4b–4d) and with the color scale spanning 200 to 450 Dobson Units (DU). A prominent polar-level TOC maximum (exceeding 400 DU) dominates the Arctic region, and this high-ozone area, related to the enhanced BDC, extends to NE China in JFM (see red curve in Figure 3a). Here, NE China in Figure 5a functions as a transition zone: its NEern section aligns with the polar high-ozone levels of ~415 DU), while the southwestern part shows a lower TOC of ~330 DU, closer to subtropical ozone levels (~300 DU; [42]). The uneven TOC distribution in the NE China region in JFM that combines polar and subtropical levels is noteworthy. Figure 5(b) displays the corresponding 2015–2024 TOC climatology for the JAS (July–September) season, with a compressed color scale (200 to 340 DU) that reflects the seasonal ozone minimum (red curve in Figure 3a). During JAS, TOC across NE China is notably more uniform compared to JFM, with TOC stabilizing around 300 DU, which is somewhere around the minimum level among the mid-latitude regions (Figure 3b). This creates a stark seasonal contrast: JFM marks the regional ozone maximum associated with BDC, while JAS represents the regional ozone minimum due to weakened ozone transport and enhanced photochemical loss.

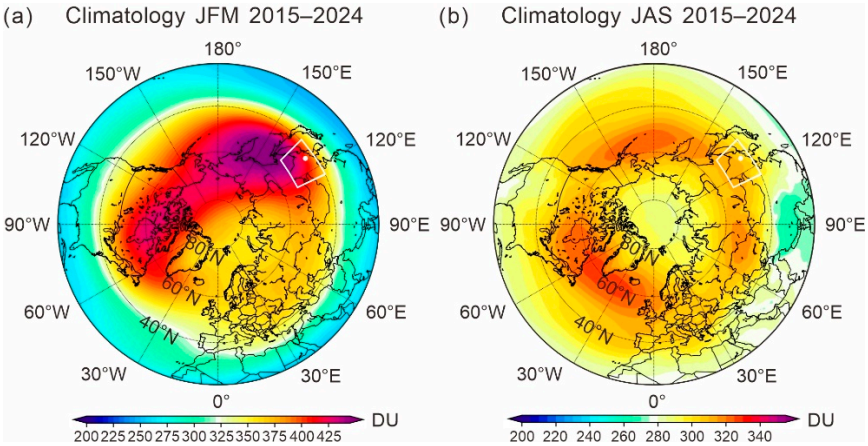

Figure 5. 10-year climatology TOC for JFM and JAS in the Northern Hemisphere, the white dot represents the Longfengshan Station.

Figure 6 displays the spatial distribution of NH TOC for January, February and March of each year from 2015 to 2024, with the blue box delineating NE China (consistent with the regional boundary defined in prior analyses). Across all these January–March panels, the TOC within the NE China domain consistently falls within the higher TOC range (per the color scale, typically ≥400 DU), an observation that aligns with the conclusion that JFM represents the annual peak in ozone levels for this region (Figure 3a). This high TOC level is maintained despite the overall high variability of the TOC pattern over mid- and high latitudes (Figure 6). In contrast, localized areas (e.g., parts of the Arctic) exhibit far more pronounced interannual variability in TOC distribution, with some years showing distinct low-ozone patches (2016, 2020 and 2022 in Figure 6).

Despite the interannual fluctuations in ozone distribution across surrounding or remote regions, the maximum TOC levels in NE China remain relatively stable throughout the 2015–2024 January–March period. With no substantial deviations from its typical high TOC state, this contrasts to low-TOC appearance in Arctic noted above. The consistent, high-stability TOC in this region during JFM is mainly associated with the pattern of the TOC maximum in the high latitudes due to the intense BDC and its persistent penetration to the NE China region.

 doi:10.20944/preprints202603.1235.v1

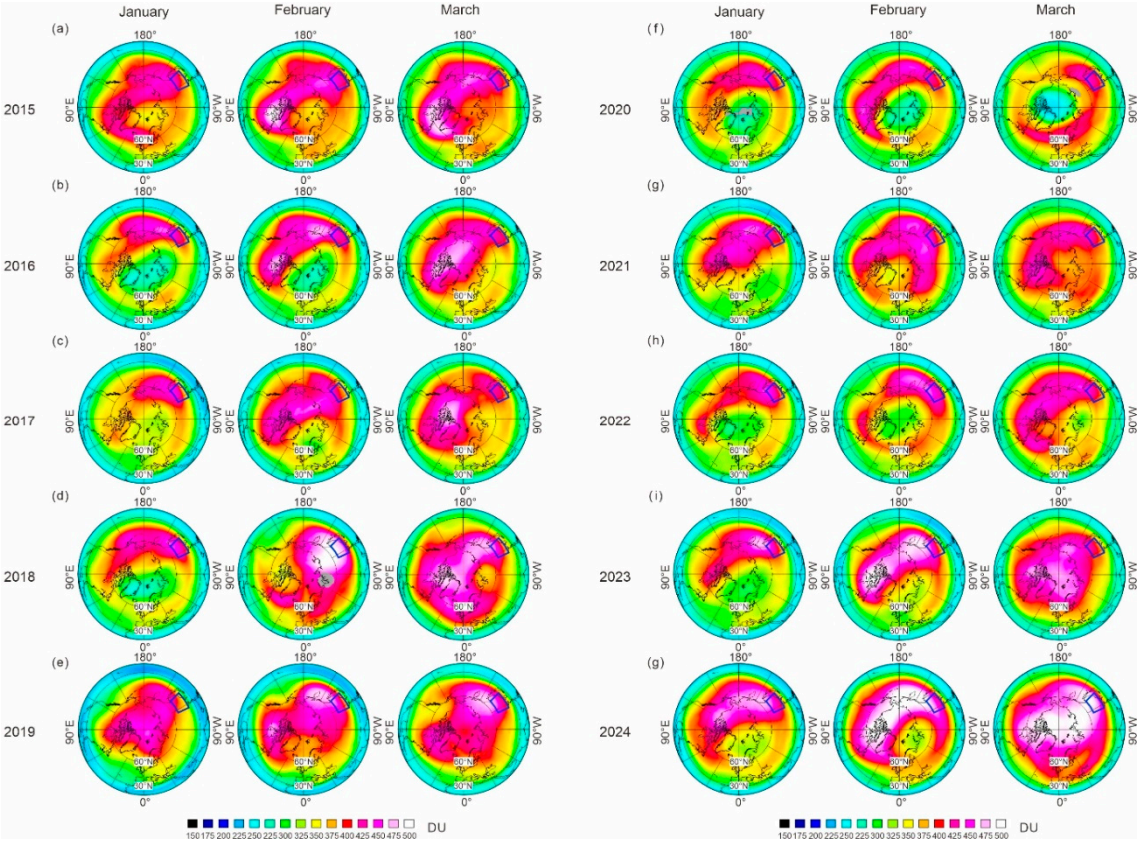

Figure 6. Total ozone column (January–March) in the Northern Hemisphere from 2015 to 2024.

This condition further serves as a critical seasonal baseline for subsequent investigations into the large-scale and regional drivers of NE China's ozone dynamics.

3.4. Longfengshan Station

The TOC data at Longfengshan Station (44.7°N, 127.6°E, 334 m a.s.l.), a NE China-based site (marked with a red dot in Figure 1), was retrieved from the World Ozone and Ultraviolet Radiation Data Centre (WOUDC) platform. Figure 7 illustrates TOC variability and regional representativeness at this station from Jan 2015 to Mar 2022: Figure 7a depicts daily TOC fluctuations, showing high-frequency variability (200–550 DU) and clear seasonal peaks/troughs over the 7-year period; Figure 7b compares monthly mean TOC values (blue dots, Longfengshan; red dots, NE China regional average); Figure 7c quantifies the monthly difference between NE China and Longfengshan as green dots, with a dashed zero line to highlight deviation direction.

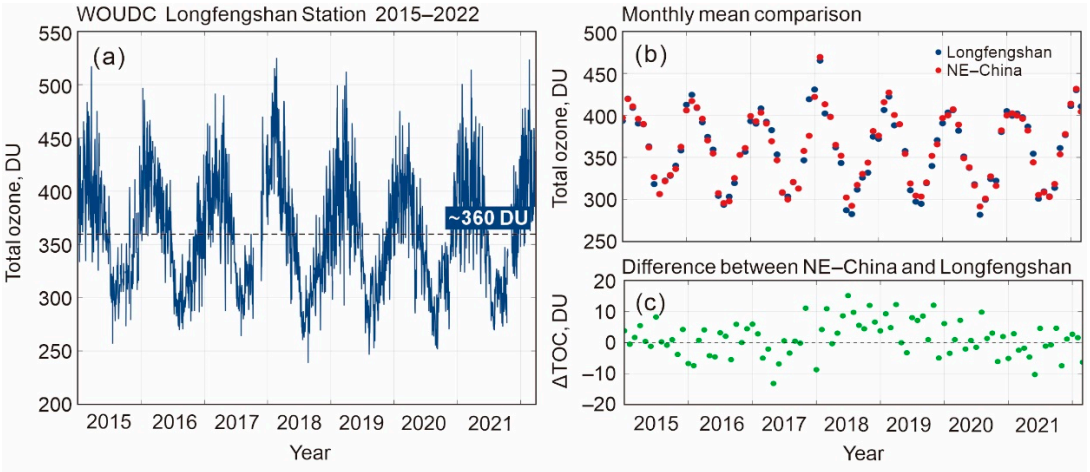

 doi:10.20944/preprints202603.1235.v1

Figure 7. (a) TOC at Longfengshan Station from Jan 2015 to Mar 2022; (b) monthly mean TOC of Longfengshan Station (blue dots) and NE China (read dots); (c) monthly difference between the regional and station-based monthly means.

Consistent with the broader NE China region (dashed line in Figure 7), Longfengshan Station's TOC data exhibit a high degree of quantitative coincidence in overall temporal variations. A pronounced seasonal cycle is evident across all datasets, with elevated TOC values in winter and spring and depressed values in summer and autumn. Notably, the monthly mean differences between the target region and Longfengshan Station remain within ±15 DU (±4.2%) of a 7-year annual mean throughout the study period (Figure 7c), validating the station's reliability as a representative proxy for regional TOC levels. Summer differences tend to be positive (indicating slightly higher regional concentrations), while winter differences are negative or near-zero, reflecting subtle seasonal disparities in ozone distribution between the site and the broader region. Over the 7-year span, no significant long-term increasing or decreasing trend is detected in either the station or regional TOC data, indicating that natural interannual and seasonal variability dominates the observed fluctuations.

3.5. Ozone Concentration

Figure 8(a) displays the pressure–time cross-section of the zonal mean ozone concentration (from the ERA-5 dataset, 2015–2024) for 40–53°N. The horizontal axis covers the years 2015 to 2024, while the vertical axis represents pressure (ranging from 1 to 1000 hPa, in logarithmic scale), with the color bar quantifying ozone concentration (units: 10^{12} cm^{-3}). A dashed horizontal line marks the 50 hPa stratospheric level: across all years, ozone concentration peaks near this 50 hPa level (reaching values close to 9×10^{12} cm^{-3}), whereas it remains relatively low (typically < 3×10^{12} cm^{-3}) in the lower tropospheric range (around 1000 hPa) and at the stratopause level (near 1 hPa), revealing distinct vertical stratification of ozone distribution.

Figure 8(b) illustrates the variation of Pearson correlation coefficients *r* between NE China TOC and zonal mean ozone concentration with pressure. The vertical axis also uses pressure and the horizontal axis spans *r* values from –0.75 to 1, with the red shaded area denoting a strong positive correlation ($r > 0.8$). The correlation coefficient fluctuates between about –0.5 and 0.7 in the tropospheric pressure range (e.g., 300–1000 hPa), but rises sharply to exceed 0.8 in the lower-stratospheric pressure region (corresponding to the red area, about 30–200 hPa), indicating a significant and strong positive linkage between TOC and ozone concentration in this stratospheric pressure range.

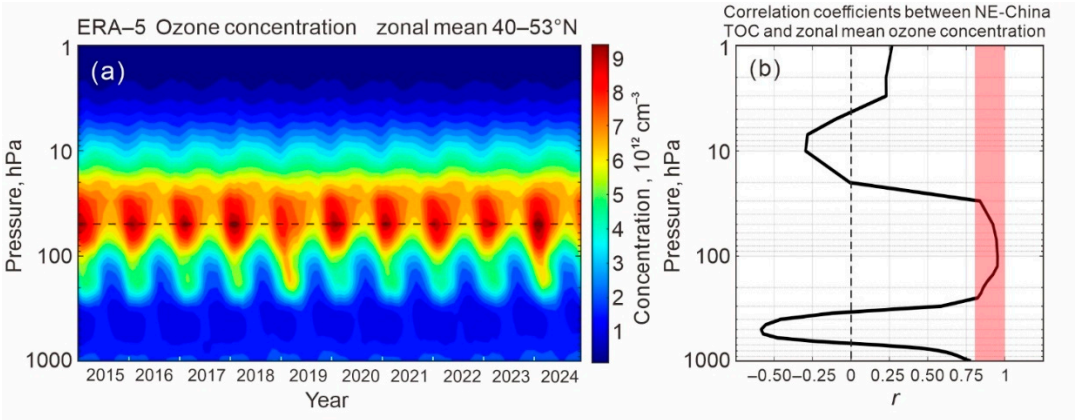

Figure 8. (a) The ozone concentration at zonal mean 40–53°N region in pressure–time section for 2015–2024. Dashed horizontal lines mark the stratosphere level at 50 hPa (black, maximum level); (b) Variation of Pearson correlation coefficients between NE China TOC and zonal mean ozone concentration with pressure. The red area represents high positive correlation (>0.8).

 doi:10.20944/preprints202603.1235.v1

Correlation decreases in the middle and upper stratosphere at the pressure levels <30 hPa, however values near $r = -0.25$ and $r = 0.25$ in annual variations (Figure 8b) are statistically significant at the 99% confidence level (Table 1).

Table 1. Pearson correlation coefficients between NE China TOC and zonal mean ozone concentration (OC). The values significant at the 99% confidence level are in bold.

Correlation coefficient	*r* (TOC-OC1)	*r* (TOC-OC10)	*r* (TOC-OC50)	*r* (TOC-OC100)	*r* (TOC-OC500)	*r* (TOC-OCsurf)
Annual	**0.27**	**–0.29**	**0.92**	**0.95**	**–0.58**	**0.78**
Winter	–0.10	**0.61**	**0.69**	**0.72**	0.04	0.06
Spring	**0.66**	**–0.51**	**0.63**	**0.91**	–0.36	**0.60**
Summer	**–0.81**	**0.69**	**0.92**	**0.93**	–0.07	**0.83**
Autumn	**0.83**	**–0.78**	**0.86**	**0.91**	**–0.50**	**0.76**

Table 1 displays the Pearson correlation coefficients *r* between NE China TOC and zonal mean ozone concentration (OC) across distinct vertical levels (from 1 hPa in the upper stratosphere to the surface) and seasons. Note the different criteria for the significance testing in the annual and seasonal variations due to different time series lengths. The 99% confidence level corresponds to $r = 0.23$ for $N = 120$ and $r = 0.46$ for $N = 30$, respectively. OC50 and OC100 make the largest contribution to interannual variations in TOC with correlation between $r = 0.63$ and $r = 0.95$. The role of OC50 looks somewhat weaker ($r = 0.63$ to $r = 0.92$) than OC100 ($r = 0.72$ to $r = 0.95$), although OC50 is at the peak concentration by height. Overall, the correlation coefficients in winter are generally smaller than those observed in other seasons. Notably, the lowest correlation (TOC-OC100) with $r = 0.72$ is reached in winter, increases to $r = 0.91$–0.93 in spring–autumn and maximizes annually with $r = 0.95$.

Regarding the surface level (OCsurf), the correlation coefficient in Table 1 in winter is particularly low (only $r = 0.06$, nearly negligible), but response of OCsurf to TOC noticeably increases in spring ($r = 0.60$), summer ($r = 0.83$), autumn ($r = 0.76$) and annually ($r = 0.78$). At 10 hPa 1 hPa in the middle and upper stratosphere, there exist distinct strong seasonal positive and negative correlations *r*(TOC-OC10) and *r*(TOC-OC1), and this phenomenon, along with the connection between OCsurf and TOC, deserves further study regarding seasonal variability.

3.6. Correlation Between TOC and Temperature

Figure 9 shows the monthly average temperatures across four atmospheric layers (1 hPa, 10 hPa, 100 hPa, and the surface) over the region 40–53°N, 115–135°E during 2015–2024, and Table 2 contains their correlation coefficients with TOC. The curves in Figure 9 show that the surface temperature Tsurf (reddish-orange curve) fluctuates most broadly (~260 K to ~300 K), the 1 hPa temperature T1 (blue curve) varies between ~240 K and ~270 K, the 10 hPa temperature T10 (purple curve) stays relatively stable around ~230 K, and the 50 and 100 hPa temperature, T50 and T100 (green and orange curves) remains the lowest (~210 K to ~220 K). All temperature series exhibit clear annual seasonal fluctuations, with periodic peaks and troughs matching the region's climatic cycles.

Table 2 presents Pearson correlation coefficients between the TOC and temperatures (at 1 hPa, 10 hPa, 50 hPa, 100 hPa, and surface Tsurf), as well as between Tsurf and stratospheric temperatures, shown in Figure 9 and analyzed across annual and seasonal (Winter, Spring, Summer, Autumn) scales. The correlation results, paired with the layered temperature ranges, underscore altitude-dependent dynamics. The T50 and T100 temperatures represent the coldest lower-stratospheric layers, which have a moderate to strong positive correlation with TOC, while T1, T10, and Tsurf show predominantly negative associations. Similarly to ozone concentrations in Table 1, the role of T100 in TOC variations in certain seasons, as shown in Table 2, appears to be somewhat more significant ($r = 0.59$ to $r = 0.92$), than T50 ($r = 0.58$ to $r = 0.88$).

 doi:10.20944/preprints202603.1235.v1

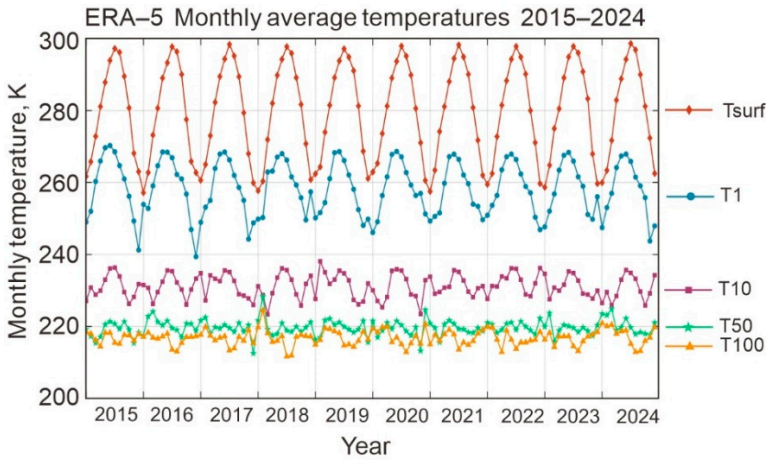

Figure 9. Monthly average temperatures at 1 hPa, 10 hPa, 50hPa, 100 hPa, and the surface (T1, T10, T50, T100, Tsurf) over the region 40–53°N, 115–135°E during 2015–2024.

Table 2. Pearson correlation coefficients between TOC and temperature over Northeast China. The values significant at the 99% confidence level are in bold.

Correlation coefficient	*r* (TOC-T1)	*r* (TOC-T10)	*r* (TOC-T50)	*r* (TOC-T100)	*r* (TOC-Tsurf)	*r* (Tsurf-T1)	*r* (Tsurf-T10)	*r* (Tsurf-T50)	*r* (Tsurf-T100)
Annual	**–0.30**	–0.14	**0.33**	**0.70**	**–0.68**	**0.84**	**0.40**	–0.04	**–0.54**
Winter	0.35	–0.13	**0.58**	**0.59**	–0.04	–0.03	–0.19	–0.10	0.06
Spring	**–0.62**	**–0.55**	0.26	0.39	**–0.74**	**0.88**	**0.57**	0.11	–0.01
Summer	**0.78**	**0.68**	**0.88**	**0.92**	**–0.59**	–0.19	–0.02	**–0.54**	**–0.70**
Autumn	**–0.84**	0.12	0.21	**0.75**	**–0.87**	**0.85**	0.07	0.14	**–0.53**

Meanwhile, surface temperature is the warmest layer (Figure 9), and there are the strong negative correlations (TOC-Tsurf) of $r = –0.68$ and (Tsurf-T100) of $r = –0.54$ in annual variations (Table 2). Consisting with (TOC-OCsurf) of $r = 0.78$ in Table 1, these results for the NE China region likely reflect interaction between the surface and lower stratosphere at a statistically significant level.

Winter stands out for its uniformly weak correlations: TOC shows only weak positive links with 1 hPa ($r = 0.35$) and negligible negative correlations with T10 ($r = –0.13$) and Tsurf ($r = –0.04$). Significant at the 99% confidence level is only correlation with T100 ($r = 0.59$) and T50 ($r = 0.58$). This is obviously due to the dominant contribution of ozone concentrations OC50 and OC100 to ozone column variability (Table 1) and well-known fact that the lower-stratospheric temperature is primarily regulated by ozone changes [21]. Tsurf has almost no meaningful associations with all upper-air temperatures ($|r| < 0.20$), making Winter the season with the lowest coherence between the variables.

4. Discussion

Based on MSR-2 satellite reanalysis data, ERA-5 reanalysis data, and ground-based observation data from Longfengshan Station during 2015–2024, this study systematically analyzed the long-term trend, seasonal variation, climatological characteristics of total ozone column (TOC) in NE China (40–53°N, 115–135°E), as well as its vertical correlation with ozone concentration and temperature. It reveals the key driving mechanisms and regional particularities of ozone distribution in mid-high latitudes.

4.1. Spatiotemporal Characteristics of TOC

There was no significant long-term change trend in TOC over NE China from 2015 to 2024, but it remained consistently higher than the zonal average level of the same latitude zone (40–53°N). This regional difference of approximately 25 DU (7.4%) was mainly contributed by the high values in

 doi:10.20944/preprints202603.1235.v1

winter (Figure 2). This phenomenon stems from the large-scale circulation regulation of ozone in mid-high latitudes. In winter, the Northern Hemisphere BDC intensifies, transporting high-concentration ozone meridionally through tropical upwelling and extratropical downwelling and influencing the vertical profile of stratospheric ozone and temperature [4]. As a transition zone between mid and high latitudes, NE China is more prominently affected by this circulation. The high-TOC patterns in the NH midlatitudes in winter–spring are formed by quasi-stationary waves (Section 1) with presence of zonal wave 1 and wave 2 [39]. The NE China region, in terms of longitude and latitude, falls climatologically at the extended TOC maximum over East Asia reaching up to 450 DU (Figure 5a). At the same time, large midlatitude sector of 30°W–90°E is filled with relatively low TOC levels of about 370–380 DU (Figure 5a). The latter circumstance lowers the zonal mean values compared to the regionally averaged ones and explains the 25-DU excess of the NE China TOC over the zonal mean TOC in Figure 2b.

The correlation coefficient between TOC in NE China and the zonal average of the same latitude zone reaches $r = 0.91$ (Section 3.1). This indicates that interannual variations in both time series are mainly dominated by global-scale atmospheric processes associated with BDC and QSW and reflected in regional processes. However, there are obvious seasonal differences: TOC in summer is close to the zonal average level (Figure 2). The large-scale circulation anomaly in winter, which causes a zonally asymmetric pattern of the TOC maximum (Figure 5a), is significantly weakened in summer, so the TOC field becomes more zonally uniform (Figure 5b). Since the BDC shuts down, intense photochemical depletion in summer, reduces ozone concentration and TOC tends to its annual minimum both in the NE China region (Figure 3a) and generally across the NH midlatitudes [4,43].

We emphasize that NE China is located in the transition zone from the polar high-ozone region to the subtropical low-ozone region (Figures 4–6). Affected by latitude gradient and circulation partitioning resulted in the QSW structure in TOC in winter, the spatial heterogeneity is significant: TOC in the NEern part can reach 415 DU under the influence of the polar TOC expansion due to the QSW structure, while that in the southwestern part is close to the subtropical level of 330 DU (Figure 5a). This is a climatological regional property in the TOC pattern, which has not previously been distinguished. During summer and autumn (JAS), TOC in the entire region is uniformly stable at around 300 DU (Figure 5b), mainly due to the BDC cessation and photochemical ozone loss, as noted above.

The seasonal fluctuation of the TOC pattern further reflects the influence of atmospheric dynamics (Figures 4 and 6). The variance and amplitude ranges in the NE China region are the largest in February (Figure 3b), corresponding to intense planetary wave activities in winter [4]. In addition, the abnormally high TOC values in the NE China region in February 2018 and March 2024 (corresponding curves in Figure 3a) increased by about 50 DU compared to the 10-year average. This is consistent with the estimate for March 2024, when Arctic TOC was 60 DU higher than the 1979–2023 average, based on Microwave Limb Sounder (MLS) data [26]. The MLS data show that this record ozone anomaly was concentrated in the lower stratosphere and can be related to extreme planetary wave events, which forced poleward and downward ozone advection into the lower stratosphere [26]. The overall consistency of the midlatitude and polar TOC anomalies confirms the special connection of the NE China region with higher latitudes through wave activity and QSW structure in TOC.

The variance is the smallest from July to October (Figure 3b), indicating the limitation of the upward wave propagation due to stable easterly stratospheric circulation during these months [4]. This speculation needs to be further verified by combining more observational and model data.

During 2015–2022, the local ground-based observation data from Longfengshan Station were highly consistent with the satellite-derived average TOC in NE China (Figure 7b), with the monthly average difference always controlled within ±15 DU (Figure 7c), verifying the reliability of MSR-2 satellite data in this region. The consistency between station and satellite data demonstrates the effective characterization capability of satellite reanalysis data for the spatiotemporal variation of regional ozone, but there are subtle seasonal differences: the regional average TOC in summer is

 doi:10.20944/preprints202603.1235.v1

slightly higher than the observed value at Longfengshan Station, while it is close to or slightly lower in winter (Section 3.4). This may be due to the location of the station relative to the climatological TOC field, which has a tendency for seasonal redistribution of the TOC level in the NE China region (Figure 5).

4.2. Correlations Between TOC, Ozone Concentration and Temperature

The vertical structure of ozone shows that the zonal average ozone concentration in 40–53°N reaches a peak in the stratosphere at 50 hPa (Figure 8a), while the concentration in the troposphere and upper stratosphere is significantly lower. This is consistent with the photochemical mechanism of stratospheric ozone formation [44] and the winter increase in ozone concentration in the lower stratosphere due to the strong seasonal cycle in the BDC and the associated enhanced winter ozone transport [4]. The TOC is significantly positively correlated with ozone concentration in the stratospheric region of 30–200 hPa ($r > 0.8$, Figure 8b), confirming that TOC variation is mainly contributed by the lower-stratospheric ozone. The correlation between ozone concentration and TOC shows obvious dependence on altitude with alternating sign changes: if the lower-stratospheric ozone is significantly positively correlated with TOC up to $r = 0.7–0.8$, then the mid-tropospheric ozone at 400–600 hPa becomes negatively correlated reaching $r = –0.5$ and the near-surface temperature is again in positive coupling with $r = 0.75$ (Figure 8b).

The correlation in the middle stratosphere is lower ($r = –0.25$), opposite in sign to the correlation in the upper stratosphere ($r = 0.25$), but, as noted in Section 3.5, is still statistically significant at the 99% confidence level. In short, there are two atmospheric layers where TOC in the NE China is positively (negatively) coupled with the interannual variability in the zonal mean ozone concentration. This altitude dependence of the correlation is partially contributed by the vertical ozone profile in the stratosphere due to the photochemistry and BDC, as well as the tropospheric contamination, but a detailed analysis of these processes is beyond the scope of this work.

As follows from r-values in Table 1, the ozone concentration at the 100-hPa pressure level (OC100) makes the largest contribution to interannual variations in TOC, despite the maximum OC is at 50 hPa (Figure 8a). The same dominance of layer 100 hPa relative to layer 50 hPa is also found in correlations between TOC and stratospheric temperature (Table 2). This dominance is observed in all seasons and is generally consistent with the difference in the range of ozone anomaly variability between the lower and middle–upper stratosphere.

By Chipperfield et al. [45], time series of ozone anomaly for 1998–2017, averaged from 60°S–60°N, show approximately twice as much variation in the lower stratosphere than in middle and upper stratosphere. A similar difference between ozone anomalies at 50 hPa and 125 hPa was observed over Europe in 1979–2004 [46]. It should be noted that the relative role of the lower-stratosphere pressure levels in the TOC variations has not previously been addressed. The relationship between the correlations in Tables 1 and 2 indicates that the ozone maximum at 50 hPa ($6–9×10^{12}$ cm^{-3}, Figure 8a) is a smaller contributor to TOC than ozone at 100 hPa ($3–6×10^{12}$ cm^{-3}).

Most changes in stratospheric ozone are associated with dynamic processes [45], however, they may have different relative importance at 50 hPa and 100 hPa. The 50-hPa level (maximum ozone concentration in the vertical profile) may be more sensitive to ozone variability associated with its downwelling from upper levels due to the BDC transport [4]. In contrast, the 100-hPa level (16 km) is closer to the tropopause, which, through the evolution of tropospheric pressure systems, can elevate or descend and affect ozone abundance here, while the tropopause shift effect becomes negligible near the ozone maximum at 50–30 hPa (20–25 km; [47]). Because of seasonal change in dynamical disturbances (e.g., winter–spring BDC intensification and winter maximum in cyclone–anticyclone frequency), the dominant correlative coupling between TOC and OC100/T100 in all seasons can not be fully explained in this limited discussion and should include a more complete further analysis of altitudinal difference in contributing sources.

Correlations between the surface and stratospheric temperatures in Table 2 indicate their significant coupling, both negative (100 hPa and 50 hPa) and positive (10 hPa and 1 hPa) in individual

 doi:10.20944/preprints202603.1235.v1

seasons. This type of temperature interaction was analyzed in the recent case studies of the stratosphere impact on extreme weather events [48,49]. Our results for 2015–2024 in Tables 1 and 2 show that the surface and stratosphere can be interdependent with statistically significant correlations between the monthly mean time series. This finding implies additional opportunities in the study of weather and climate change.

The low correlation between TOC and OCsurf in winter (Table 1) suggests that stratospheric intrusions play a negligible role in modulating surface ozone variations over NE China, even though such intrusions and TOC both peak in winter [29,30]. Since TOC variability is dominated by ozone at 50 hPa and 100 hPa in the lower stratosphere, the wintertime lower stratosphere cannot be regarded as a primary source for surface ozone changes. In contrast, surface ozone exhibits a pronounced seasonal maximum in spring and summer, which is mainly driven by in situ photochemical production and regional precursor emissions rather than stratospheric downward transport [27,28]. The prominent maximum correlation coefficients in Table 1 during spring–autumn likely reflect the combined effects of intensified photochemical activity, favorable meteorological conditions for ozone formation, and relatively stable stratosphere–troposphere exchange in these seasons. These processes are consistent with the dominant role of tropospheric photochemistry and regional dynamical transport in regulating surface ozone over East Asia, as documented in previous studies [29,30].

5. Conclusions

This study analyzes the variations and trend of total ozone column (TOC) over NE (NE) China spanning 2015 to 2024 and using the Multi-Sensor Reanalysis Version 2 (MSR-2) dataset, with key findings closely linked to the Brewer–Dobson Circulation (BDC), a quasi-steady meridional circulation in the stratosphere that drives tropical lower-stratospheric ascent, poleward transport, and extratropical stratospheric descent. A central finding from this analysis is that the TOC over NE China in winter consistently remains higher than that observed in zonal means within the same latitude band. This pattern is likely shaped by the BDC's poleward transport of ozone-rich air and persistent expansion of the high polar TOC into the midlatitude NE China due to the quasi-stationary wave (QSW) structure. The weakening of wave activity and BDC due to easterly circulation in the stratosphere in summer and early autumn, combined with photochemical ozone loss, results in seasonal TOC minimum.

The main findings in this work can be summarized as follows:

1) The TOC over NE China shows no statistically significant linear trend throughout the period 2015–2024. The excess of annual mean TOC in the study region relatively the zonal mean TOC is about 25 DU (7.4%) and is contributed mainly by the higher winter TOC values, whereas the minimum TOC values in summer are close and do not affect the difference. The strong correlation between the regional and zonal mean TOC with $r = 0.91$ suggests that the annual TOC dynamics in NE China is mainly driven by large-scale atmospheric processes.

2) Seasonal cycle demonstrates TOC maximum (minimum) in February (August) occurring one month (two months) earlier than typically in the NH midlatitudes.

3) In winter and spring, the increased TOC in NE China is tightly coupled with the extended high-latitude TOC maximum due to the QSW structure, implying the dominance of enhanced ozone transport, associated with BDC during these seasons, not only in the Arctic, but also in the study region of midlatitudes.

4) As a transition zone between the polar and subtropical latitudes, NE China in climatology for January–March 2015–2024 combines the highest TOC levels of ~415 DU in the NE part of the region and the lowest TOC of ~330 DU in the southwestern (SW) part. The NE–SW direction of significant TOC decrease is a characteristic feature of the TOC distribution over NE China in winter and spring, which should be taken into account when analyzing ozone observations and studying the stratosphere–troposphere coupling.

5) The ground-based observations at Longfengshan Station in 2015–2022 closely match MSR-2 data averaged over NE China. The monthly mean difference varies within ±15 DU (±4.2% of a 7-year

 doi:10.20944/preprints202603.1235.v1

annual mean), validating the station's reliability as a representative proxy for regional TOC variability.

6) The stratospheric ozone concentrations (OCs) at 50 hPa and 100 hPa are main contributors to monthly mean TOC variability over NE China in 2015–2024. It is important that the correlations of TOC with the 50-hPa OC maximum (OC50) is systematically lower than with OC100 in all of four seasons. The highest difference is in spring with r = 0.63 and r = 0.91, respectively. The distinct importance of the two close pressure levels in the TOC variations may indicate a weaker variability of ozone downwelling above 50 hPa due to the BDC compared to the change in the partial ozone column below 100 hPa due to the tropopause effect associated with tropospheric pressure systems.

7) The surface ozone concentration (OCsurf) in the region is negligibly correlated with TOC in in winter (only r = 0.06), but significantly correlated in spring (r = 0.60), summer (r = 0.83), autumn (r = 0.76) and annually (r = 0.78). Since TOC is supplied mainly by the lower-stratospheric ozone, correlative relationships indicate strong and positive dependence of OCsurf on the stratospheric ozone in spring–autumn. Moreover, Tsurf has a similar significant but negative relationship with TOC, demonstrating the close stratosphere–surface interaction in the NE China region, which has been poorly investigated previously.

These findings enrich the understanding of ozone distribution dynamics in East Asian mid-latitudes, particularly highlighting how the effects of BDC, QSW and the tropopause may underpin the unique TOC traits of NE China relative to its latitudinal counterparts. However, the specific ways in which different factors interact over the region to provide significant stratosphere–surface coupling, remain to be explored. Future research will combine more site-based observational data with the MSR-2 dataset to investigate the underlying mechanisms in depth, including refining the analysis of links between Longfengshan Station data, regional TOC, BDC transport processes, QSW pattern and the response of the tropopause to tropospheric pressure anomalies. Such efforts will provide more robust support for a comprehensive understanding of ozone dynamics in East Asian mid-latitudes.

Author Contributions: Conceptualization, methodology, investigation and interpretation, O.E., Y.S. and G.M.; data acquisition, software, related figures and visualization, O.E. and Y.S.; validation, writing—original draft preparation, writing—review and editing, O.E., Y.S. and G.M.; supervision and project administration, G.M. Each author contributed to the interpretation and discussion of the results and edited the manuscript. All authors have read and agreed to the published version of the manuscript.

Funding: This research was funded by Heilongjiang University, Harbin, China, grant number 2025-KYYWF-ZR0423.

Data Availability Statement: Data will be made available on request.

Acknowledgments: Monthly mean TOC data are from the Multi-Sensor Reanalysis Version 2 (MSR-2) at https://www.temis.nl/protocols/o3field/o3mean_msr2.php. Ozone concentrationi and air temperaturei at selected pressure levels are derived from the European Centre for Medium-Range Weather Forecasts (ECMWF) ERA-5 dataset (https://cds.climate.copernicus.eu/datasets/reanalysis-era5-pressure-levels?tab=overview). The Longfengshan Station data are used from the World Ozone and Ultraviolet Radiation Data Centre (WOUDC) platform (https://woudc.org/en/data/stations/?id=326&lang=en).

Conflicts of Interest: The authors declare no conflicts of interest.

Abbreviations

The following abbreviations are used in this manuscript:

TOC	Total Ozone Column
BDC	Brewer–Dobson Circulation
QSW	Quasi-Stationary Wave
DU	Dobson Units

 doi:10.20944/preprints202603.1235.v1

ERA-5	ECMWF Reanalysis Version 5
MSR-2	Multi-Sensor Reanalysis Version 2
NE China	Northeast China
NH	Northern Hemisphere
OC	Ozone Concentration
DJF	December, January and February
JJA	June, July and August
JFM	January, February and March
JAS	July, August and September

References

1. Grant, W.B. Solar Ultraviolet Radiation and Mortality from Skin Cancer: An Ecological Study. *Science* **1988**, *242*, 1111–1112. https://doi.org/10.1126/science.3187538.
2. Diffey, B.L. Climate Change, Ozone Depletion and the Impact on Ultraviolaaet Exposure of Human Skin. *Phys. Med. Biol*. **2004**, *49*, R1–R11. https://doi.org/10.1088/0031-9155/49/1/R01.
3. Lucas, R.M.; Takizawa, Y.; Rhodes, L.E.; Yazar, S.; Young, A.R.; Norval, M.; de Gruijl, F.R.; Sinclair, C.A.; Neale, R.E. Human Health in Relation to Exposure to Solar Ultraviolet Radiation Under Changing Stratospheric Ozone and Climate. *Photochem. Photobiol. Sci.* **2019**, *18*, 641–680. https://doi.org/10.1039/c8pp90060d.
4. Shepherd, T.G. Transport in the Middle Atmosphere. *J. Meteor. Soc. Japan.* **2007**, *85B(3)*, 165–191. https://doi.org/10.2151/jmsj.85B.165.
5. Wang, Y.; He, Y.; Sheng, Z.; Sun, J.; Qin, Z.; Tao, Y. Vertical Ozone Transport by Rossby Wave Breaking in Upper Troposphere-Lower Stratosphere Is Weakening. *Atmos. Environ.* **2025**, *343*, 120999. https://doi.org/10.1016/j.atmosenv.2024.120999.
6. Shepherd, T.G.; McLandress, C. A robust mechanism for strengthening of the Brewer–Dobson circulation in response to climate change. *J. Atmos. Sci*. **2011**, *68(4)*, 784–797. https://doi.org/10.1175/2010JAS3608.1.
7. Bozhkova, V.; Liudchik, A., Umreiko, S. Long-term trends of total ozone content over mid-latitudes of the Northern Hemisphere. *Int. J. Remote Sens*. **2019**, *40*, 5216–5229. https://doi.org/10.1080/01431161.2019.1579384.
8. Chen, Z.; Xie, Y.; Liu, J.; Shen, L.; Cheng, X.; Han, H.; Yang, M.; Shen, Y.; Zhao, T.; Hu, J. Distinct seasonality in vertical variations of tropospheric ozone over coastal regions of southern China. *Sci. Total Environ*. **2023**, *874*, 162423. https://doi.org/10.1016/j.scitotenv.2023.162423.
9. Diallo, M.; Ern, M.; Ploeger, F. The advective Brewer–Dobson circulation in the ERA5 reanalysis: climatology, variability, and trends. *Atmos. Chem. Phys.* **2021**, *21*, 7515-7544. https://doi.org/10.5194/acp-21-7515-2021.
10. Kumar, C.; Dogra, A.; Yadav, S.; Tandon, A.; Attri, A.K. Apportionment of Long-Term Trends in Different Sections of Total Ozone Column Over Tropical Region. *Environ. Monit. Assess.* **2022**, *194*, 298. https://doi.org/10.1007/s10661-022-09980-z.
11. Boccacci, G.; Bertolin, C.; Cavazzani, S.; Siani, A.M. Multi-year Total Ozone Column Variability at Three Norwegian Sites: Influence of Northern Hemisphere Climatic Indices. *Atmos. Environ.* **2023**, *310*, 119966. https://doi.org/10.1016/j.atmosenv.2023.119966.
12. Farman, J.C.; Gardiner, B.G.; Shanklin, J.D. Large Losses of Total Ozone in Antarctica Reveal Seasonal ClO–NO_x Interaction. *Nature* **1985**, *315*, 207–210. https://doi.org/10.1038/315207a0.
13. Hossaini, R.; Chipperfield, M.P.; Montzka, S.A.; Leeson, A.A.; Dhomse, S.S.; Pyle, J.A. The Increasing Threat to Stratospheric Ozone from Dichloromethane. *Nat. Commun.* **2017**, *8*, 15962. https://doi.org/10.1038/ncomms15962.
14. Zeng, G.; Morgenstern, O.; Williams, J.H.T.; O'Connor, F.M.; Griffiths, P.T.; Keeble, J.; Deushi, M.; Horowitz, L.W.; Naik, V.; Emmons, L.K.; Abraham, N.L.; Archibald, A.T.; Bauer, S.E.; Hassler, B.; Michou, M.; Mills, M.J.; Murray, L.T.; Oshima, N.; Sentman, L.T.; Tilmes, S.; Tsigaridis, K.; Young, P.J. Attribution of Stratospheric and Tropospheric Ozone Changes Between 1850 and 2014 in CMIP6 Models. *J. Geophys. Res. Atmos.* **2022**, *127*, e2022JD036452. https://doi.org/10.1029/2022JD036452.

 doi:10.20944/preprints202603.1235.v1

15. Velders, G.J.M.; Andersen, S.O.; Daniel, J.S.; Fahey, D.W.; McFarland, M. The Importance of the Montreal Protocol in Protecting Climate. *Proc. Natl. Acad. Sci. U. S. A.* **2007**, *104*, 4814–4819. https://doi.org/10.1073/pnas.0610328104.
16. Chipperfield, M.P.; Bekki, S.; Dhomse, S.; Harris, N.R.P.; Hassler, B.; Hossaini, R.; Steinbrecht, W.; Thiéblemont, R.; Weber, M. Detecting Recovery of the Stratospheric Ozone Layer. *Nature* **2017**, *549*, 211–218. https://doi.org/10.1038/nature23681.
17. Egorova, T.; Sedlacek, J.; Sukhodolov, T.; Karagodin-Doyennel, A.; Zilker, F.; Rozanov, E. Montreal Protocol's impact on the ozone layer and climate. *Atmos. Chem. Phys.*, **2023**, *23*, 5135–5158. https://doi.org/10.5194/acp-23-5135-2023.
18. Friedel, M.; Chiodo, G.; Sukhodolov, T.; Rozanov, E.; Egorova, T. Weakening of Springtime Arctic Ozone Depletion with Climate Change. *Atmos. Chem. Phys.* **2023**, *23*, 10235–10254. https://doi.org/10.5194/acp-23-10235-2023.
19. Sofieva, V.F.; Szelag, M.E.; Kramarova, N.; Damadeo, R.; Steinbrecht, W.; Petropavlovskikh, I.; Vigouroux, C.; Maillard Barras, E.; Zawada, D.; Tourpali, K.; Frith, S.M.; Wild, J.D.; Davis, S.M.; Arosio, C.; Weber, M.; Rozanov, A.; Auffarth, B.; Froidevaux, L.; Fuller, R.; Degenstein, D.; Dube, K.; Effertz, P.; Leblanc, T.; Ancellet, G.; Godin-Beekmann, S.; McConville, G.; Querel, R.; Smale, D.; DeBacker, M.-R.; Mahieu, E.; Sussmann, R. Updated Global and Regional Trends of Stratospheric Ozone Profiles. *EGUsphere* **2025**, https://doi.org/10.5194/egusphere-2025-5963.
20. Kuttippurath, J.; Kumar, P.; Nair, P.J.; Pandey, P.C. Emergence of Ozone Recovery Evidenced by Reduction in the Occurrence of Antarctic Ozone Loss Saturation. *npj Clim. Atmos. Sci.* **2018**, *1*, 42. https://doi.org/10.1038/s41612-018-0052-6.
21. Zhou, L.; Xia, Y.; Zhao, C. Influence of Stratospheric Ozone Changes on Stratospheric Temperature Trends in Recent Decades. *Remote Sens.* **2022**, *14*, 5364. https://doi.org/10.3390/rs14215364.
22. Hu, D.Z.; Tian, W.S.; Xie, F.; Wang, C.X.; Zhang, J.K. Impacts of Stratospheric Ozone Depletion and Recovery on Wave Propagation in the Boreal Winter Stratosphere. *J. Geophys. Res. Atmos.* **2015**, *120*, 8299–8317. https://doi.org/10.1002/2014JD022855.
23. Lozitsky, V.; Grytsai, A.; Klekociuk, A.; Milinevsky, G. Influence of Planetary Waves on Total Ozone Column Distribution in Northern and Southern High Latitudes. *Int. J. Remote Sens.* **2011**, *32*, 3179–3186. https://doi.org/10.1080/01431161.2010.541519.
24. Zhang, J.; Tian, W.; Xie, F.; Li, Y.; Wang, F.; Huang, J.;Tian, H. Influence of the El Niño southern oscillation on the total ozone column and clear-sky ultraviolet radiation over China. *Atmos. Environ.* **2015**, *120*, 205–216. https://doi.org/10.1016/j.atmosenv.2015.08.080.
25. Shin, D.; Oh, Y.-S.; Seo, W.; Chung, C.-Y.; Koo, J.-H. Total Ozone Trends in East Asia from Long-Term Satellite and Ground Observations. *Atmosphere* **2021**, *12*, 982. https://doi.org/10.3390/atmos12080982.
26. Newman, P.A.; Lait, L. R.; Kramarova, N.A.; Coy, L.; Frith, S.M.; Oman, L.D.; Dhomse, S.S. 2024 Arctic Total Column Ozone. *Geophys. Res. Lett.* **2024**, *51*, e2024GL110924. https://doi.org/10.1029/2024GL110924.
27. Jing, P.; Banerjee, S. Rossby Wave Breaking and Isentropic Stratosphere-Troposphere Exchange During 1981–2015 in the Northern Hemisphere. *J. Geophys. Res. Atmos.* **2018**, *123*, 9011–9025. https://doi.org/10.1029/2018JD028997.
28. Li, D.; Bian, J.C.; Fan, Q.J. A deep stratospheric intrusion associated with an intense cut-off low event over East Asia. *Sci. China Earth Sci.* **2015**, *58*, 116–128. https://doi.org/10.1007/s11430-014-4977-2.
29. Wang, H.Y.; Wang, W.K.; Shangguan, M.; Wang, T.Y.; Hong, J.; Zhao, S.Y.; Zhu, J.T. The Stratosphere-to-Troposphere Transport Related to Rossby Wave Breaking and Its Impact on Summertime Ground-Level Ozone in Eastern China. *Remote Sens.* **2023**, *15*, 2647. https://doi.org/10.3390/rs15102647.
30. Zhu, F.R.; Luo, J.L.; Wang, Z.H.; Jin, H.; Zhao, Q.F.; Wang, Z.T.; Luo, F.H.; Gu, M.Z. The Impact of Stratosphere-to-Troposphere Transport Associated with the NE China Cold Vortex on Surface Ozone Concentrations in Eastern China. *J. Appl. Meteorol. Climatol.* **2024**, *63*, 1241–1253. https://doi.org/10.1175/JAMC-D-24-0027.1.

 doi:10.20944/preprints202603.1235.v1

31. Yu, R.; Grytsai, A.; Milinevsky, G.; Evtushevsky, O.; Klekociuk, A.; Shi, Y.; Poluden, O.; Wang, X.; Ivaniha, O. Zonal Asymmetry in Ozone Variations Over Antarctic Stations During the Life Cycle of Sudden Stratospheric Warmings. *J. Geophys. Res. Atmos.* **2025**, *130*, e2024JD042896. https://doi.org/10.1029/2024JD042896.
32. Zhang, J.; Tian, W.; Xie, F.; Chipperfield, M.P.; Feng, W.; Son, S.-W.; Abraham, N.L.; Archibald, A.T.; Bekki, S.; Butchart, N.; Deushi, M.; Dhomse, S.; Han, Y.; Jöckel, P.; Kinnison, D.; Kirner, O.; Michou, M.; Morgenstern, O.; O'Connor, F.M.; Pitari, G.; Plummer, D.A.; Revell, L.E.; Rozanov, E.; Visioni, D.; Wang, W.; Zeng, G. Stratospheric Ozone Loss Over the Eurasian Continent Induced by the Polar Vortex Shift. *Nat. Commun.* **2018**, *9*, 206. https://doi.org/10.1038/s41467-017-02565-2.
33. Collins, W.J.; Derwent, R.G.; Garnier, B.; Johnson, C.E.; Sanderson, M.G.; Stevenson, D.S. Effect of Stratosphere-Troposphere Exchange on the Future Tropospheric Ozone Trend. *J. Geophys. Res. Atmos*. **2003**, *108*, 8528. https://doi.org/10.1029/2002JD002617.
34. Tang, C.; Zhu, F.; Wei, Y.; Tian, X.; Yang, J.; Zhao, F. Study of Time-Frequency Domain Characteristics of the Total Column Ozone in China Based on Wavelet Analysis. *Atmosphere* **2023**, *14*, 941. https://doi.org/10.3390/atmos14060941.
35. Meng, X.; Jiang, J.; Chen, T.; Zhang, Z.; Lu, B.; Liu, C.; Xue, L.; Chen, J.; Herrmann, H.; Li, X. Chemical Drivers of Ozone Change in Extreme Temperatures in Eastern China. *Sci. Total Environ.* **2023**, *874*, 162424. https://doi.org/10.1016/j.scitotenv.2023.162424.
36. Meng, K.; Zhao, T.L.; Bai, Y.Q.; Wu, M.; Cao, L.; Hou, X.W.; Luo, Y.H.; Jiang, Y.C. Tracing the Origins of Stratospheric Ozone Intrusions: Direct vs. Indirect Pathways and Their Impacts on Central and Eastern China in Spring–Summer 2019. *Atmos. Chem. Phys.* **2024**, *24*, 12623–12642. https://doi.org/10.5194/acp-24-12623-2024.
37. Chen, J.; Sun, L.; Jia, H.; Li, C.; Ai, X.; Zang, S. Effects of Seasonal Variation on Spatial and Temporal Distributions of Ozone in NE China. *Int. J. Environ. Res. Public Health* **2022**, *19*, 15862. https://doi.org/10.3390/ijerph192315862.
38. Gao, C.; Xiu, A.; Zhang, X.; Chen, W.; Liu, Y.; Zhao, H.; Zhang, S. Spatiotemporal Characteristics of Ozone Pollution and Policy Implications in NE China. *Atmos. Pollut. Res.* **2020**, *11*, 357–369. https://doi.org/10.1016/j.apr.2019.11.008.
39. Zhang, C.; Evtushevsky, O.; Milinevsky, G.; Klekociuk, A.; Andrienko, Y.; Shulga, V.; Han, W.; Shi, Y. The Annual Cycle in Mid-Latitude Stratospheric and Mesospheric Ozone Associated with Quasi-StationaryWave Structure by the MLS Data 2011–2020. *Remote Sens.* **2022**, *14*, 2309. https://doi.org/10.3390/rs14102309.
40. van der A, R.J.; Allaart, M.A.F.; Eskes, H.J. Extended and refined multi sensor reanalysis of total ozone for the period 1970–2012. *Atmos. Meas. Tech.* **2015**, *8*, 3021–3035. https://doi.org/10.5194/amt-8-3021-2015.
41. Hersbach, H.; Bell, B.; Berrisford, P.; Hirahara, S.; Horányi, A.; Muñoz-Sabater, J.; Nicolas, J.; Peubey, C.; Radu, R.; Schepers, D.; Simmons, A.; Soci, C.; Abdalla, S.; Abellan, X.; Balsamo, G.; Bechtold, P.; Biavati, G.; Bidlot, J.; Bonavita, M.; Chaira, G.; Dahlgren, P.; Dee, D.; Diamantakis, M.; Dragani, R.; Fleming, J.; De Forbes, R.; Fuentes, M.; Geer, G.; Haimberger, L.; Healy, S.; Hogan, R.J.; Hólm, E.; Janisková, M.; Keeley, S.; Laloyaux, P.; Lopez, P.; Lupu, C.; Radnoti, G.; de Rosnay, P.; Rozum, I.; Vamborg, F.; Villafuerte, L.; Thépaut, J. The ERA5 Global Reanalysis. *Q. J. R. Meteorol. Soc.* **2020**, *146*, 1999–2049. https://doi.org/10.1002/qj.3803.
42. Coldewey-Egbers, M., Loyola, D.G., Labow, G., and Frith, S.M. Comparison of GTO-ECV and adjusted MERRA-2 total ozone columns from the last 2 decades and assessment of interannual variability. *Atmos. Meas. Tech.* **2020**, *13*, 1633–1654. https://doi.org/10.5194/amt-13-1633-2020.
43. Zhang, X.Y.; Sun, J.M.; Lin, W.L.; Xu, W.Y.; Zhang, G.; Wu, Y.L.; Dai, X.; Zhao, J.R.; Yu, D.J.; Xu, X.B. Long-Term Variations in Surface Ozone at the Longfengshan Regional Atmosphere Background Station in NE China and Related Influencing Factors. *Environ. Pollut*. **2024**, *348*, 123748. https://doi.org/10.1016/j.envpol.2024.123748.
44. Dütsch, H.U. The Ozone Distribution in the Atmosphere. *Can. J. Chem.* **1974**, *52(8)*, 1491–1504. https://cdnsciencepub.com/doi/10.1139/v74-220.

 doi:10.20944/preprints202603.1235.v1

45. Chipperfield, M.P., Dhomse, S., Hossaini, R., Feng, W., Santee, M.L., Weber, M., Burrows, J.P., Wild, J.D., Loyola, D., Coldewey-Egbers, M. On the cause of recent variations in lower stratospheric ozone. *Geophys. Res. Lett.* **2018**, *45*. https://doi.org/10.1029/2018GL078071.
46. Terao, Y., Logan, J.A. Consistency of time series and trends of stratospheric ozone as seen by ozonesonde, SAGE II, HALOE, and SBUV(/2). *J. Geophys. Res. Atmos.* **2007**, *112*, D06310. https://doi.org/10.1029/2006JD007667.
47. Steinbrecht, W., Claude, H., Köhler, U., Hoinka, K.P. Correlations between tropopause height and total ozone: Implications for long-term changes. *J. Geophys. Res.* **1998**, *103*, 19183–19192. https://doi.org/10.1029/98JD01929.
48. Xiong, X., Liu, X., Wu, W., Knowland, K.E., Yang, F., Yang, Q., Zhou, D.K. Impact of stratosphere on cold air outbreak: Observed evidence by CrIS on SNPP and its comparison with models. *Atmosphere* **2022**, *13*, 876. https://doi.org/10.3390/atmos13060876.
49. Shi, Y., Evtushevsky, O., Milinevsky, G., Yu, R., Grytsai, A., Sun, X., Wang, X., Novosyadlyj, B. Extreme cooling in NE China in January and concurrent maximum in the lower stratospheric temperature and ozone: Case studies. *Atmos. Environ.* **2025**, *342*, 120938, https://doi.org/10.1016/j.atmosenv.2024.120938.